Testing for Welding, Joining or Additive Manufacturing Applications

Mustafa Engin Kocadağistan*, Oğuzhan Çinar and Tanju Teker

Weldability and mechanical behavior of CMT welded AISI 430 and HARDOX 500 steels

https://doi.org/10.1515/mt-2023-0169
Published online June 29, 2023

Abstract: In this study, AISI 430 and HARDOX 500 steels were joined by cold metal transfer (CMT) welding method. The properties and microstructural changes of the welding and HAZ regions were investigated by OM and SEM analyses. Microhardness, notch impact, and tensile tests were performed to determine the mechanical properties of the welded specimens. The ruptured surfaces of the test specimens after the impact test were examined using SEM. Coarse grains were formed in the HAZ regions but were limited to the low-temperature input of the cold metal transfer welding. The N3 specimen was broken from AISI 430 base metal and the elongation amount was 16.32 mm. Tensile strengths were from 380 to 493 MPa. The mechanical properties of AISI 430 and HARDOX 500 steels combined with CMT welding increased significantly and weldability was proven possible.

Keywords: cold metal transfer; hardness; mechanical; microstructure; steels; welding

1 Introduction

In parallel with the technological development, high strength steels have become very important in many branches of industry. The most important point here is that these steels can be welded with each other. Many welding techniques are used for this purpose. The CMT (cold metal transfer) technique, which is a MIG/MAG process, has gained more importance among these techniques nowadays. The CMT welding developed by Fronius provides many advantages in terms of preserving the mechanical properties of the material types used during welding. During the welding processes, it has 30 % less heat input than the other gas metal arc welding methods [1]. The CMT technique aims to reduce spatter and heat input during welding and to minimize damage to the base metals joined by welding and it is a dip arc process, which is a droplet detachment from the wire. Due to the controlled droplet transfer, the process is known as no-spatter [2]. Both the welded materials and the weld zones are cooler than the gas metal arc welding method. It has many advantages over other welding techniques (e.g.; more precise processing with low heat input and distortion, high-quality weld bead, burr-free work, the ability to weld materials and galvanized sheets thinner than 0.3 mm, and the possibility of joining steel and aluminum) [3].

AISI 430 steels, which are included in the ferritic group, are a low-carbon stainless steel material containing 16–18 wt% Cr. Due to the different elements in its composition, its weldability is limited. The steels of type 430 do not contain nickel and molybdenum. They are not highly resistant to corrosion. It has medium machinability and is named 1.4016 or X6Cr17 according to the EN norm [4, 5]. Due to the formation of grain growth in the HAZ region, the toughness of ferritic stainless steels such as AISI 430 decreases after welding, and they are susceptible to intergranular corrosion. Therefore, special precautions must be taken during welding [6]. HARDOX steels have high toughness, bendability, and features of good weldability. For this reason, it provides a longer life of materials in areas where abrasion is intense (for example, due to its load-bearing purpose and high wear resistance feature) [7, 8]. They are abrasion resistant due to their hardness properties. Thanks to their toughness properties, it provides the advantages such as flexibility, formability, and weldability without crack formation. They are more resistant to hydrogen cracking as they have low carbon equivalent compared to other high-strength steels. Austenitic stainless steel filler materials such as AWS 307 or AWS 309 can be used for the welding operation of HARDOX-type steels [9]. In another study, HARDOX 450 and AISI 430 steels are welded using a double-sided TIG (tungsten inert gas) welding method, and the changes in chemical structure and phase characterization of welded joints were examined. No physical defects were detected in the welded joint. Pepper-

***Corresponding author: Mustafa Engin Kocadağistan**, Metallurgy and Materials, Ataturk Universitesi Muhendislik Fakultesi, Engineering Faculty, 25240, Erzurum, Türkiye, E-mail: mengink@atauni.edu.tr
Oğuzhan Çinar, Metallurgy and Materials, Ataturk Universitesi Muhendislik Fakultesi, Engineering Faculty, 25240, Erzurum, Türkiye
Tanju Teker, Manufacturing Engineering, Sivas Cumhuriyet Universitesi, Sivas Cumhuriyet Üniversitesi-Teknoloji Fakültesi- İmalat Mühendisliği Bölümü, 2892, 58140, Sivas, 253, Türkiye

like chrome carbides and grain boundary carbides were determined in HAZ-AISI 430, and acicular ferrite, widmanstädten ferrite, and martensite were determined in HAZ-HARDOX 450 [10]. In a study where AISI 430/AISI 1030 steels were welded using synergistic GMAW (manual gas metal arc) and GMAW-P (controlled impact) welding methods, the HAZ of steel joints welded with GMAW-P had narrower than that of GMAW and the steel welded with GMAW. The joints had less grain growth than the HAZ. GMAW-P welded joints of different steels had superior tensile strength and hardness than GMAW [11]. AISI 430 and HARDOX 450 steels were welded in another study using a double-sided tungsten inert gas welding method. The mixture of AISI 430 steel containing Cr and Ni and HARDOX 450 formed new phases such as Cr_7C_3, Cr_3Ni_3, $C_{23}C_6$, martensite, and $Cr_{1.36}$ $Fe_{0.52}$ in the weld metal. It was determined that the composition and amount of martensite and carbides depend on the welding heat output and rate of cooling [12, 13]. In general, ferritic stainless steels cannot be characterized by good weldability. Wires made of austenitic stainless steels are usually applied to join ferritic materials because of the good mechanical resistance, tenacity, and flexibility reached by austenitic weld metal. There were always losses of alloying elements due to the presence of O_2/CO_2, but the intensity depended on the amount of titanium/niobium [14].

In this study, AISI 430 and HARDOX 500 steels were joined by cold metal transfer (CMT) welding. The mechanical behaviors and metallography of the welding and HAZ regions of these steels were investigated.

2 Experimental approach

In this study, 130 × 100 × 10 mm AISI 430 and HARDOX 500 steels, and AWS 307 1.2 mm wire were selected for the welding process. The mechanical properties and chemical compositions of these materials are given in Tables 1 and 2.

Table 2: Chemical composition of AWS 307 welding wire (wt%).

Product quality	C	Si	Mn	Cr	Ni
AWS 307	0.08	1.45	6.62	19.10	9.03

The specimens to be welded were first cut into pieces of 130 × 100 × 10 mm with the metal cutting band saw. Then, a "V" shaped welding groove was opened to these specimens and they were centered with a gap of 2 mm between the specimens. Specimens were welded with the Fronius-Tps500i welding machine using the robotic CMT method. Welding operations were carried out with AWS 307 1.2 mm wire in 6 passes. The specimens were welded with 0° torch angle, 45 cm min^{-1} feed rate, Arco 2.5 gas, and 5.4 cm min^{-1} wire feed speed conditions. Three specimens as N1, N2, and N3 were prepared for each test and each of the specimens was welded at 120, 130, and 140 A currents, respectively. 97.5 % Argon and 2.5 % CO_2 gas were used as shielding gas. The specimens to be used for the experiments were then cut from the welded specimens with a metal band saw (Figure 1). The specimen surfaces were sanded with grit sandpaper in a sanding machine. The specimens were polished with 3 µm diamond paste on the polishing felt. In order to determine the microstructural differences that occur during the welding process, the HARDOX 500 specimen was etched with 98 % ethyl alcohol and 2 % nitric acid. AISI 430 specimen was etched in an electrolytic etching device in 49 % ethyl alcohol, 49 % hydrochloric acid, and 2 % nitric acid with a 12 V etching unit. The specimens prepared for metallographic examination were observed with an Nikon LV 150 brand optical microscope (OM) and QUANTA – FEG 250 brand scanning electron microscope (SEM). The phase changes and compounds in the welded joint zone and the HAZ were determined by a Cu-Kα beam source with a wavelength of λ = 1.5405 Å in the XRD device. The hardness values were measured at 0.5 mm intervals with a 100 g load with the SHIMADZU HMV-G brand microhardness device.

Table 1: Chemical compositions and mechanical properties of HARDOX 500 and AISI 430 steels.

Product quality	Elements and their maximum values (wt%)									
	C	Si	Mn	Al	P	S	Cr	Ni	Mo	B
HARDOX 500	0.27	0.50	1.60	–	0.025	0.01	1.20	0.25	0.25	0.005
AISI 430	0.05	0.28	0.48	0.011	–	–	16.9	0.16	0.2	–
	Hardness (HV)		Yield strength (MPa)		Tensile strength (MPa)		Notch impact resistance		Stretching (%)	
HARDOX 500	525		1400		1550		37		10	
AISI 430	172		318		490		22		18	

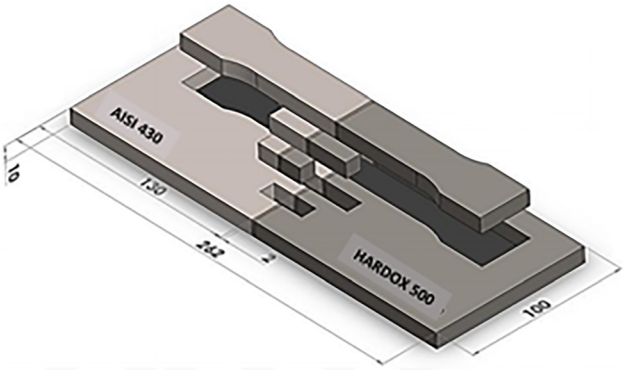

Figure 1: Removal of welded specimens.

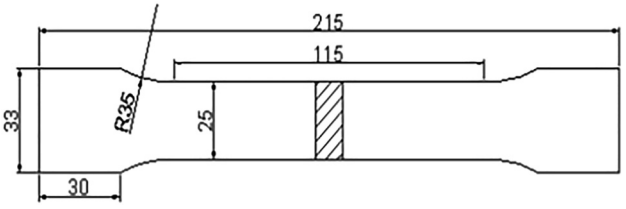

Figure 2: Tensile specimen view.

The tensile test specimens were cut with a band saw from the welded joint according to the ASTME8M-04 standard (Figure 2) [15]. Tensile tests were carried out in the SHIMADZU brand hydraulic tensile device with 100 KN tensile capacity. The specimens to be used for the measurement of the fracture energies of the welded joints were prepared according to the ASTME23-06 standard [16]. Notch impact tests were determined using a 300 J hammer in the impact testing machine. Then, the morphology of the fractured surfaces of the specimens was determined by SEM analysis.

3 Results and discussion

The macro structures of the N1, N2, and N3 specimens obtained by welding with the CMT method were examined. The weld seam width of the N3 specimen was determined to be wider than the N2 and N1 specimens. The macrostructure showed that the weld seam width increased as the current increased (Figure 3). Sectional views of N1, N2, and N3 specimens are given in Figure 4. Full penetration was achieved in all specimens and a "V" shaped weld seam was formed.

Before and after the welding process, the microstructure changings of ASI 430 and HARDOX 500 steels were also investigated in Figure 5. The structure of HARDOX 500 steel consisted of pearlite (α+Fe_3C), while the structure of AISI 430 steel consisted of a ferrite (α) phase. In AISI 430 steel, the

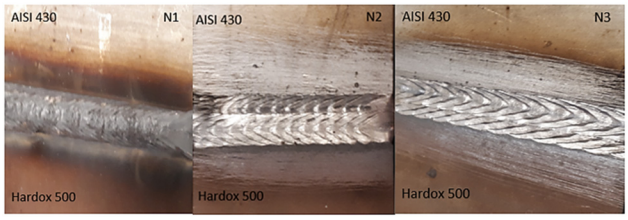

Figure 3: View of the macrostructures of the welded metal pair.

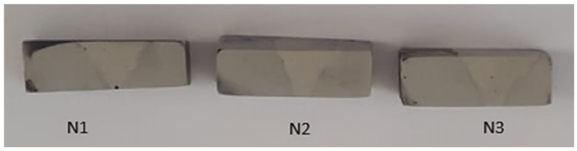

Figure 4: Macrostructure images of the intersections of N1, N2, and N3 specimens.

white-colored phases consist of ferrite (α), and the looking darker parts consist of textures.

The weld metal microstructure of the welded steel pairs is given in Figure 6. There was a dendritic structure in the weld zone. The welded structure consisted of austenite (γ) and delta ferrites (δ). It has been reported that the presence of delta ferrites in certain proportions improved the mechanical properties because it absorbed impurities in the metal [17]. Finer particles, lower heat input, and higher cooling rates are formed in the weld zone in similar studies belonging to the welded joints made with the CMT method [18].

Figure 7 shows the schematic view of the HAZ zones of the AISI 430 and HARDOX 500 steels welded by the CMT technique. It is known that the heat generated during welding will direct to the metal with high thermal conductivity. A represents AISI 430 steel and H symbolizes HARDOX steel. A4 is the coarse-grain zones, A3 is the finer-grain zones. A2 represents the partially transition zones, while A1 represents the heat-unaffected zones. Likewise, H4 schematizes high temperature, H3 medium temperature, H2 low temperature, and H1 heat-unaffected zones. *K* represents the weld metal zone. Since the thermal conductivity of AISI 430 metal is lower than HARDOX 500, the HAZ region is narrower.

The coarse grained HAZ region formed right next to the weld metal in the AISI 430 region is shown in Figure 8. Grain boundary and intragranular carbides were seen in the enlarged microstructure. The cooling rate increased with increasing current intensity, intense lath-type carbides, peppery-carbides in the grain, and grain boundary carbides were formed. The coarse-grained formation during the welding process in the HAZ region is the normal state [10].

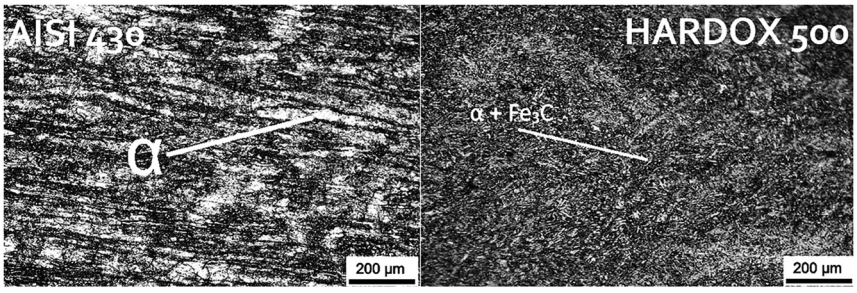

Figure 5: Microstructure of AISI 430, HARDOX 500, before welding.

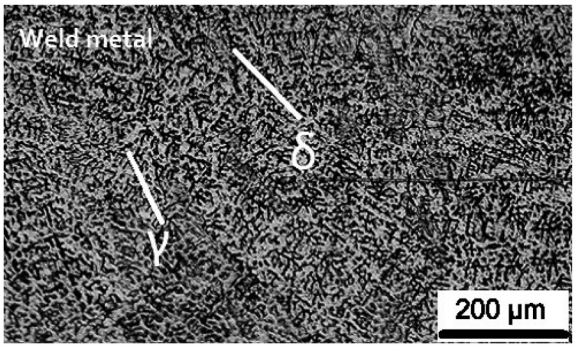

Figure 6: Weld metal microstructure of the welded steel pairs.

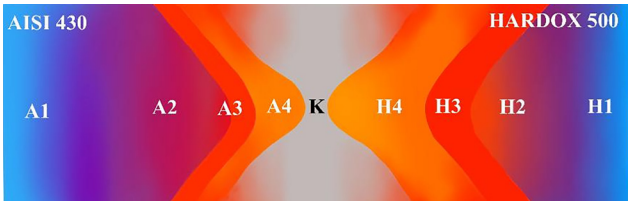

Figure 7: AISI 430 and HARDOX 500 steels and heat affected zones.

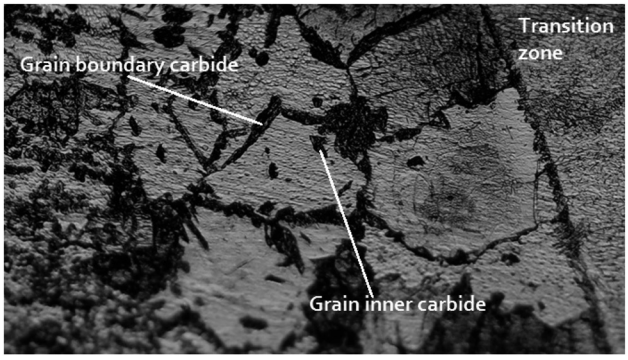

Figure 8: Microstructure of AISI 430-HAZ.

A larger HAZ region was formed in the microstructure of the HARDOX 500 region compared to AISI 430 (Figure 9). Acicular ferrite and widmanstatten ferrite formations were also seen in the HAZ zone due to heat inputs during welding. Partially more acicular ferrite was formed in the microstructure of the N3 specimen compared to the microstructure of the N1 specimen. This situation can also be associated with an increase in the cooling rate as the current increases. With the increase in the cooling rate, lath-type martensitic structures and more acicular ferrite structures were formed in the HAZ [10].

When the micro images of the AISI 430-part of the N1, N2, and N3 specimens are examined, it is seen that the coarse-grained part of the N1 specimen in the HAZ zone is narrower than the other specimens, and the coarse-grained region grew further with the increase of the current. There was no significant difference in the widths of the HAZ regions of the N1 and N3 specimens. The HAZ regions of the N3 and N2 specimens were wider than the HAZ region of the N1 specimen (44 % and 29 %, respectively). There was a direct proportionality between the increase in current and the relative grain coarsening. The optical image of the N3 specimen welded at 140 A given in Figure 10 and SEM images are given in Figure 11. In studies comparing traditional MIG/MAG welding and CMT welding, when welding with CMT, it was stated that the peppery-carbides occur in grains of the AISI 430-HAZ region, finer grains and more ferrite are formed in the welding seam. The formation of peppery-carbides was due to the carbides formed during cooling [18, 19]. The increase in the cooling rate when the current increased created a coarser dendritic structure in the microstructure of the weld metal. No cracks were observed in any of the welded joints.

SEM-EDS analysis of N3 specimen was given in Figure 12. The maximum values of Fe, C, Ni, Mn, Cr, Si, and Mo amounts were determined as 89.90 wt%, 14.72 wt%, 9.31 wt%, 22.07 wt%, 22.09 wt%, 3.55 wt%, and 0.67 wt% at different points of HARDOX 500 region, respectively. The minimum values of Fe, C, Ni, Mn, Cr, Si, and Mo amounts in AISI430 side were determined as 59.06 wt%, 1.24 wt%, 0.43 wt%, 0.77 wt%, 0.18 wt%, 0.22 wt%, and 0.05 wt% at different points of AISI 430 region, respectively. Fe, Cr, Mn, Ni, Mo, C, and Si elements were detected in both the weld metal and the base metal. The elements in the weld metal of the AISI 430-HAZ side were more than those in the HARDOX 500-HAZ side. The reason for this can be explained by the atomic density. In similar studies, there were atomic transitions from high

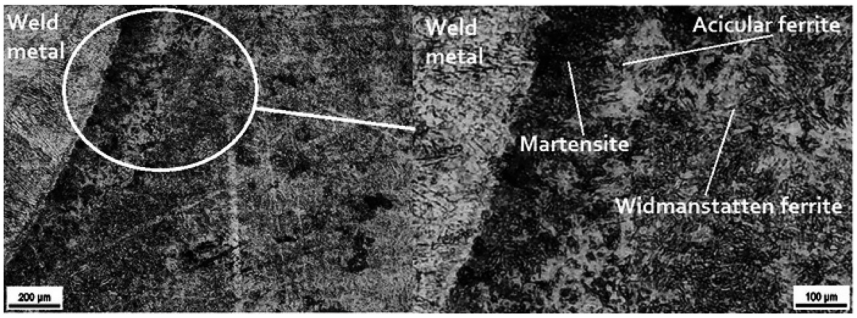

Figure 9: Microstructure of HARDOX 500-HAZ.

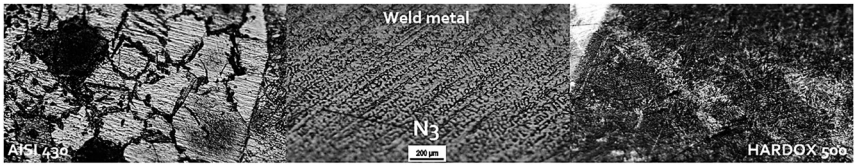

Figure 10: Optical microstructure of the N3 specimen.

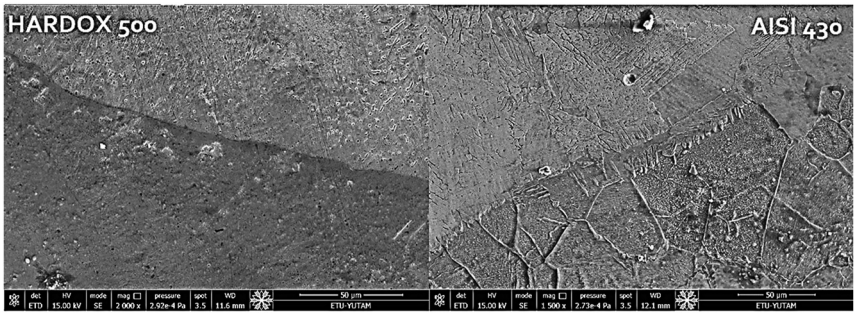

Figure 11: SEM view of the N3 specimen.

atomic density to low atomic density [10]. The element transitions increased between the HAZ zone and the weld metal zone with the increasing current intensity.

Microhardness graphic of specimens are showed in Figure 13. The highest hardness in the weld metal was measured as N3 = 538 HV. While the austenitic structure in the weld metal had a higher hardness than AISI 430-base metal, it had lower hardness values than HARDOX 500-base metal. It is thought that the carbide precipitation in the weld metal increases the hardness [20]. A decrease in hardness values was observed in the transition from the AISI 430-base metal to the AISI 430-HAZ zone. This was due to carbides formed in the grain inner and grain boundary zone despite grain coarsening. Nickel and manganese mixed with the base metals from the weld metal reduced the formation of chromium-carbide. A general decrease in the hardness values was observed in the transition from the HARDOX 500-base metal to the HARDOX 500-HAZ zone. This situation was caused by tempered martensite [21, 22]. The causes of the reduction in hardness and tensile strengths were slower cooling and coarse grain microstructures. Nagasai et al. [18] revealed that the grain size was reduced due to the wire retraction mechanism of the CMT process, which reduced heat input and increased cooling rate.

The impact energies of the specimens were determined as N1 = 99.99 J, N2 = 118.43 J, and N3 = 128.9 J. The macro images of the specimens are given in Figure 14. All of the specimens were fractured from the weld zone where the notch was opened. SEM images taken from the specimen surfaces as a result of the notch impact test are given in Figure 15. The surfaces were ductile and had a spongy structure [23].

The EDS graphic of the fractured surface of the N3 specimen are given in Figure 16. In general, the amounts of Fe, Cr, Mn, and Ni were high. It is known that manganese has the effect of increasing hardness and decreasing fracture toughness.

The macro images of the specimens after the tensile test are given in Figure 17. In the tensile test server, the tensile strength values of the N1, N2, and N3, were measured respectively as 380 MPa, 486 MPa, and 493 MPa. The maximum elongation amounts of N1, N2, and N3 specimens were calculated as 5.11 mm, 15.27 mm, and 16.32 mm, respectively. After the tensile test, the N1 specimen was fractured by the side of AISI 430 of the weld area. The reason for this is the

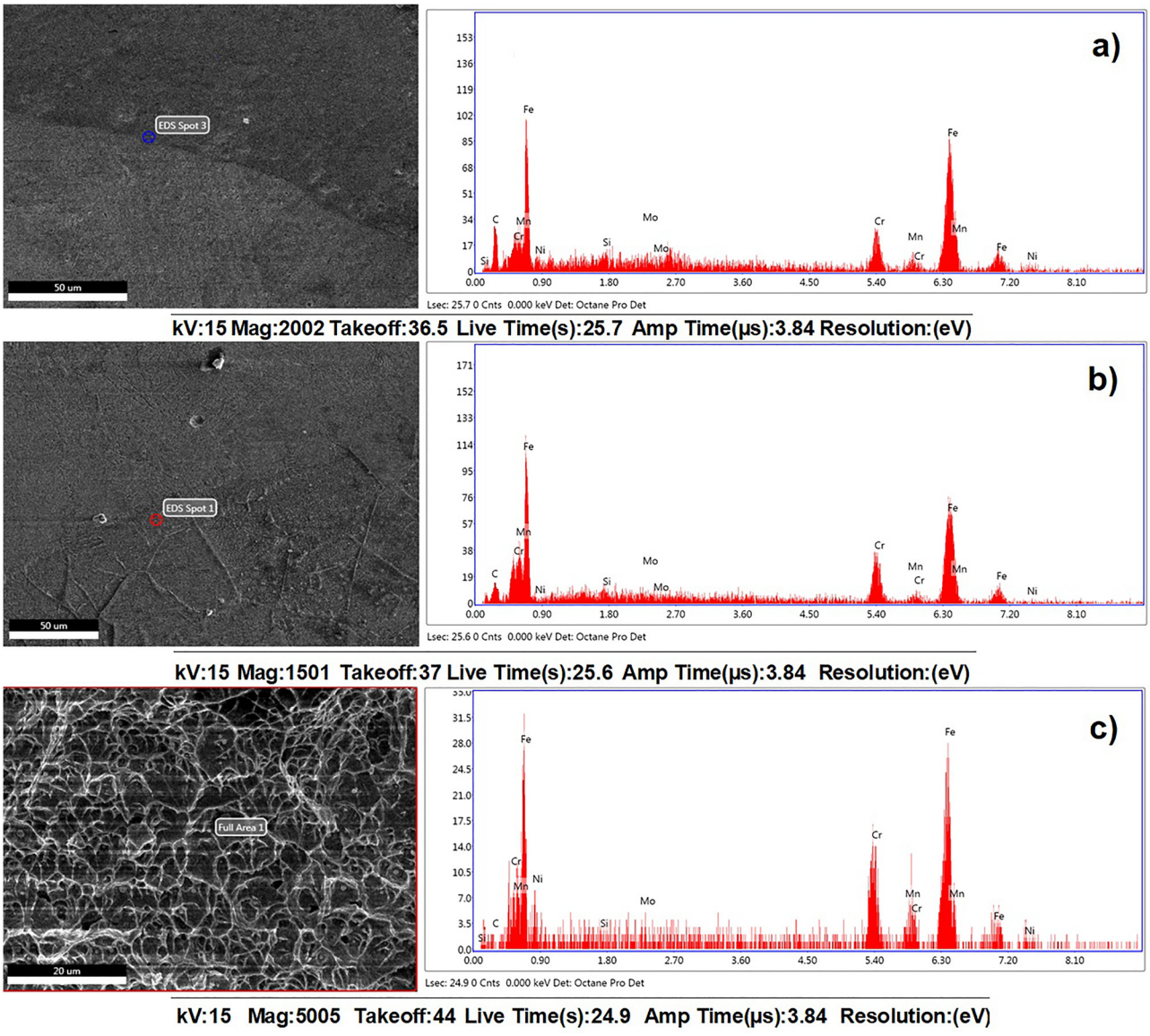

Figure 12: SEM/EDS graphics, a) SEM/EDS graphic of the HARDOX 500 HAZ region of the N3, b) SEM/EDS graphic of the AISI 430 region of the N3, and c) SEM/EDS graphic of the weld metal region of the N3.

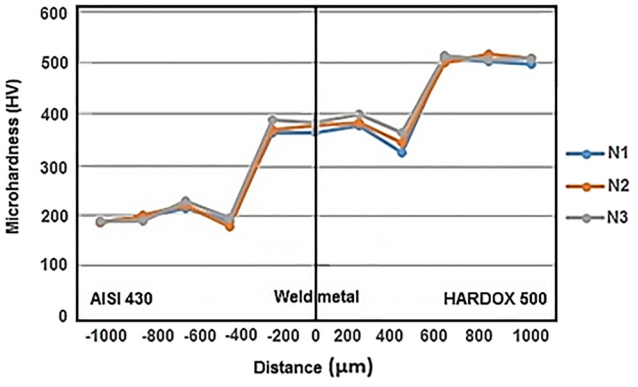

Figure 13: Microhardness graphic of specimens.

precipitation of chromium carbides in the HAZ zone and the grain coarsening occurs when they pass from the liquid phase to the solid ferrite phase. This is thought to may also be due to low penetration [24].

The N2 and N3 specimens were fractured from the side of AISI 430-base metal. The austenite additional wire prevents the formation of intermetallic phases in the weld metal and reduces carbide formation in the AISI 430 part [25, 26]. While N2 and N3 specimens were fractured by waisting, the N1 specimen broke without waisting in the macro dimension. When comparing the CMT welding method with the MIG welding method, the specimens welded with the CMT welding method have less distortion than the MIG welding method.

Figure 14: Fractured specimens after notch impact test.

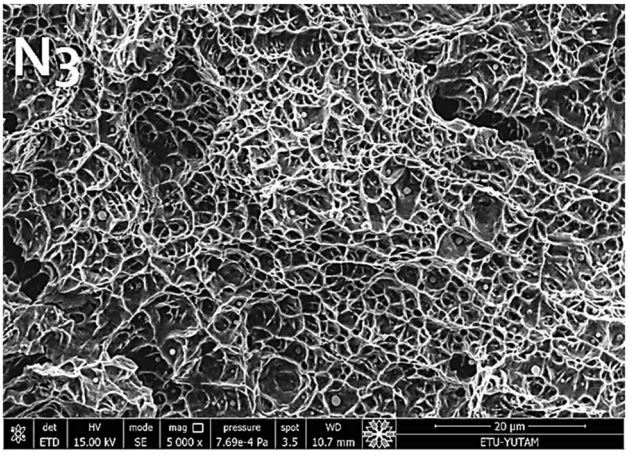

Figure 15: Fractured surface SEM image of the N3 specimen after impact test.

It was measured as N1 = 380 MPa, N2 = 486 MPa, and N3 = 493 MPa in tensile tests. N2 and N3 specimens were fractured from the base metal. Because of the use of the additional wire, the austenitic structure formed in the weld metal reduced the formation of chromium carbide and martensite and prevented the formation of intermetallic compounds [25, 26]. In the low-current welding process, there were no voids and no full joining in the N1 specimen. The tensile strength increased as the current increased.

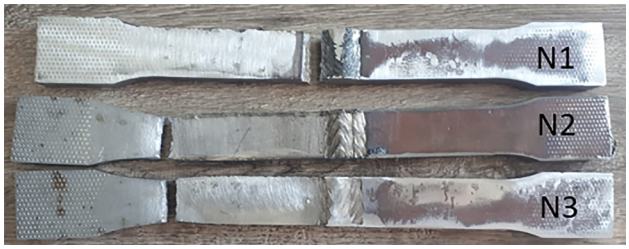

Figure 17: Macro views of N1, N2, and N3 specimens.

The phases formed in the material structure of N1, N2, and N3 specimens are given in Figure 18. Austenite, Cr_7C_3, Cr_3Ni_3, Ni phase, and compounds were detected in the structure. These phases have a rigid and brittle structure. But Nickel has a face-centered cubic structure. Therefore, it formed austenite with high toughness and increased the mechanical properties of the austenite material [10].

4 Conclusions

In this study, HARDOX 500 and AISI 430 steels with different mechanical and chemical properties were joined by the CMT welding method using additional wire. The following results were obtained.

The low heat input of CMT provided the desired grain reduction in the microstructure. Less distortion and high-quality joints occurred.

No cracks and gaps were observed in the HAZ zones of the specimens.

The highest hardness in the weld metal was measured as N3 = 538 HV. The microhardness of the welded joints decreased in the transition from weld metal to AISI 430 and HARDOX 500 metals. Martensites and chromium carbide formations detected in the weld metal had an effect on the increase in strength.

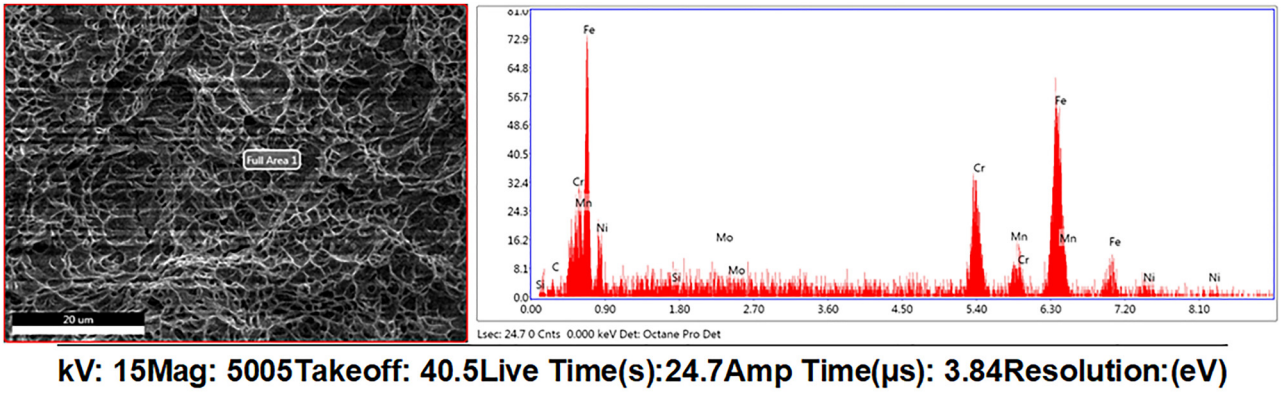

Figure 16: Fractured surface SEM and EDS graphic of the N3 specimen.

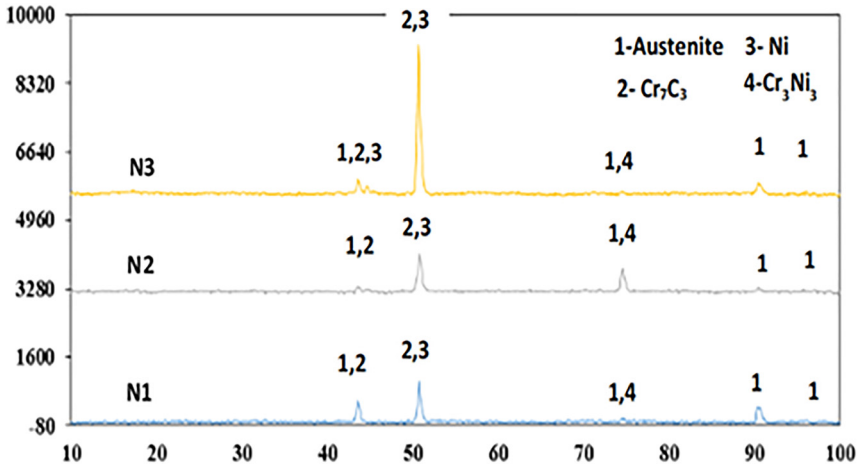

Figure 18: XRD analysis graphic of N1, N2, and N3 specimens.

Impact toughness changed from 99.9 to 128.9 J. The impact energies increased as the current increased.

The fracture surfaces showed a ductile fracture.

The N2 and N3 specimens were broken from AISI 430 base metal at 486 MPa and 493 MPa tensile strength, respectively. While the N2 specimen elongated by 15.27 mm, the elongation amount of the N3 specimen was 16.32 mm.

Acknowledgment: The authors were grateful to Research Fund of the Ataturk University for their assistance in conducting the experiments.

Author contributions: All the authors have accepted responsibility for the entire content of this submitted manuscript and approved submission.

Research funding: This work was supported by Research Fund of the Ataturk University. [Project Number: FYL-2021-9387].

Conflict of interest statement: No potential conflict of interest was reported by the authors.

References

[1] A. R. Kannan, N. S. Shanmugam, and S. Naveenkumar, "Effect of arc length correction on weld bead geometry and mechanical properties of AISI 316L weldments by cold metal transfer (CMT) process," *Mater. Today: Proc.*, vol. 18, no. 7, pp. 3916–3392, 2019, https://doi.org/10.1016/j.matpr.2019.07.331.

[2] S. Selvi, A. Vishvaksenan, and E. Rajasekar, "Cold metal transfer (CMT) technology- an overview," *Def. Technol.*, vol. 14, no. 1, pp. 28–44, 2018, https://doi.org/10.1016/j.dt.2017.08.002.

[3] P. N. Bellamkonda, M. Sudersanan, and B. Visvalingam, "Mechanical properties of wire arc additive manufactured carbon steel cylindrical component made by cold metal transferred arc welding process," *Mater. Test.*, vol. 64, no. 2, pp. 260–271, 2022, https://doi.org/10.1515/mt-2021-2051.

[4] A. K. Lakshminarayanan, K. Shanmugam, and V. Balasubramanian, "Effect of autogenous arc welding processes on tensile and impact properties of ferritic stainless steel joints," *J. Iron Steel Res. Int.*, vol. 16, no. 1, pp. 62–68, 2009, https://doi.org/10.1016/S1006-706X(09)60012-1.

[5] B. A. Salman, H. M. Ali, and S. S. Mohammed, "Influence of welding process and electrode material on the corrosion characteristics of AISI 304 and AISI 316 weldments," *Eng. Res. J.*, vol. 1, no. 45, pp. 7–12, 2020, https://doi.org/10.21608/ERJSH.2020.229960.

[6] J. C. Lippold and D. J. Kotecki, *Welding Metallurgy and Weldability of Stainless Steels*, Hoboken, New Jersey, USA, John Wiley and Sons, 2005.

[7] B. Mezrag, F. Deschaux-Beaume, and M. Benachour, "Control of mass and heat transfer for steel/aluminium joining using cold metal transfer process," *Sci. Technol. Weld. Joining*, vol. 20, no. 3, pp. 189–198, 2015, https://doi.org/10.1179/1362171814Y.0000000271.

[8] K. Bensaid, H. Dhiflaoui, H. Bouzaiene, H. Yahyaoui, and N. B. Fredj, "Effects of the cooling mode on the integrity and the multi-pass micro-scratching wear resistance of HARDOX 500 ground surfaces," *Int. J. Adv. Des. Manuf. Technol.*, vol. 113, no. 9, pp. 2865–2882, 2021, https://doi.org/10.1007/s00170-021-06719-x.

[9] Z. Zuo, M. Haowei, M. Yarigarravesh, et al., "Microstructure, fractography, and mechanical properties of Hardox 500 steel TIG-welded joints by using different filler weld wires," *Materials*, vol. 15, p. 8196, 2022, https://doi.org/10.3390/ma15228196.

[10] T. Teker and D. Gençdoğan, "Phase and chemical structure characterization in double sided TIG arc welding of HARDOX 450 and AISI 430 steel," *Cumhuriyet Sci. J.*, vol. 41, no. 4, pp. 987–994, 2020, https://doi.org/10.17776/csj.742964.

[11] T. Teker and T. Kurşun, "Weldability of AISI 430/AISI 1030 steel couples via the synergic controlled pulsed (GMAW-P) and manual gas metal arc (GMAW) welding techniques," *Mater. Manuf. Processes*, vol. 26, pp. 926–932, 2011, https://doi.org/10.1080/10426914.2011.551909.

[12] T. Maruyama, "Arc welding technology for dissimilar joints," *Weld. Int.*, vol. 17, pp. 276–281, 2003, https://doi.org/10.1533/wint.2003.3113.

[13] T. Teker and D. Gençdoğan, "Heat affected zone and weld metal analysis of HARDOX 450 and ferritic stainless steel double sided TIG-joints," *Mater. Test.*, vol. 63, no. 10, pp. 923–928, 2021, https://doi.org/10.1515/mt-2021-0022.

[14] D. Filho, V. A. Ferraresi, and A. Scotti, "Shielding gas influence on the ferritic stainless steel weldability," *J. Eng. Manufact.*, vol. 224, no. Part B, pp. 951–961, 2010, https://doi.org/10.1243/09544054JEM1631.

[15] ASTM E8M-04, *Standard Test Methods for Tension Testing of Metallic Materials*, West Conshohocken, PA, USA, ASTM International, 2004.
[16] ASTM E23-06, *Standard Test Methods for Notched Bar Impact Testing of Metallic Materials*, West Conshohocken, PA, USA, ASTM International, 2006.
[17] J. Verma, R. V. Taiwade, R. K. Khatirkar, and A. Kumar, "A Comparative study on the effect of electrode on microstructure and mechanical properties of dissimilar welds of 2205 austeno-ferritic and 316L austenitic stainless steel," *Mater. Trans.*, vol. 57, no. 4, pp. 494–500, 2016, https://doi.org/10.2320/matertrans.M2015321.
[18] B. P. Nagasai, S. Malarvizhi, and V. Balasubramanian, "Effect of welding processes on mechanical and metallurgical characteristics of carbon steel cylindrical components made by wire arc additive manufacturing (WAAM) technique," *CIRP J. Manuf. Sci. Technol.*, vol. 36, pp. 100–116, 2022, https://doi.org/10.1016/j.cirpj.2021.11.005.
[19] C. Lin, J. Liu, H. Tsai, and C. Cheng, "Evolution of microstructures and mechanical properties of AZ31B magnesium alloy weldment with active oxide fluxes and GTAW process," *J. Chin. Inst. Eng.*, vol. 34, no. 8, pp. 1013–1023, 2011, https://doi.org/10.1080/02533839.2011.618242.
[20] M. Alizadeh-Sh, S. P. H. Marashi, and M. Pouranvari, "Resistance spot welding of AISI 430 ferritic stainless steel: phase transformations and mechanical properties," *Mater. Des.*, vol. 56, pp. 258–263, 2014, https://doi.org/10.1016/j.matdes.2013.11.022.
[21] J. E. Westraadt, W. E. Goosen, A. Kostka, H. Wang, and G. Eggeler, "Modified Z-phase formation in a 12 % Cr tempered martensite ferritic steel during long-term creep," *Mater. Sci. Eng.*, vol. 855, p. 143857, 2022, https://doi.org/10.48550/arXiv.2206.15070.
[22] A. Kostka, K. G. Tak, R. J. Hellmig, Y. Estrin, and G. Eggeler, "On the contribution of carbides and micrograin boundaries to the creep strength of tempered martensite ferritic steels," *Acta Mater.*, vol. 55, no. 2, pp. 539–550, 2007, https://doi.org/10.1016/j.actamat.2006.08.046.
[23] T. Teker, "The effect of austenitic interlayer on microstructure and mechanical behaviors in keyhole plasma transfer arc welding of ferritic stainless steel couple," *Int. J. Adv. Des. Manuf. Technol.*, vol. 69, no. 5, pp. 1833–1840, 2013, https://doi.org/10.1007/s00170-013-5158-8.
[24] P. Sathiya, S. Aravindan, and A. Noorul Haq, "Effect of friction welding parameters on mechanical and metallurgical properties of ferritic stainless steel," *Int. J. Adv. Des. Manuf. Technol.*, vol. 31, no. 11, pp. 1076–1082, 2007, https://doi.org/10.1007/s00170-005-0285-5.
[25] C. H. Muralimohan and V. Muthupandi, "Friction welding of type 304 stainless steel to Cp titanium using nickel interlayer," *Adv. Mater. Res.*, vol. 794, pp. 351–357, 2013, https://doi.org/10.4028/www.scientific.net/AMR.794.351.
[26] T. Teker, "Effect of melt-in and key-hole modes on the structure and mechanical properties of AISI 430 steel welded using plasma transfer arc welding," *Phys. Met. Metallogr.*, vol. 119, no. 7, pp. 669–677, 2018, https://doi.org/10.1134/S0031918X18070116.

The authors of this contribution

Mustafa Engin Kocadağistan
Dr. Mustafa Engin Kocadağistan, born in 1965, works at the University of Ataturk, Faculty of Engineering, Department of Metallurgy and Materials Engineering, Erzurum, Turkey. He graduated in Mining Engineering from the Technical University of İstanbul, Turkey, in 1989. He received his MSc and PhD degrees from Ataturk University, Erzurum, Turkey, in 2015. He studied open-pit chrome mining, bioleaching and hydrometallurgy techniques, solid-state welding methods, boron ores, and nature restoration in open-pit mining.

Oğuzhan Çinar
Oğuzhan Çinar, born in 1985, works at the State Railways Erzurum Directorate, Erzurum, Turkey. He graduated in Metallurgy Education from Yıldız Technical University, İstanbul, Turkey, in 2014. He received his MSc degree from Ataturk University, Erzurum, Turkey, in 2022. He has been continuing his doctorate education in Ataturk University, Department of Metallurgy and Materials Engineering since 2023. He studied fusion welding methods.

Tanju Teker
Prof. Dr. Tanju Teker, born in 1971, works at the University of Sivas Cumhuriyet, Faculty of Technology, Department of Manufacturing Engineering, Sivas, Turkey. He graduated in Metallurgy Education from Gazi University, Ankara, Turkey, in 1997. He received his MSc and PhD degrees from Firat University, Elazig, Turkey, in 2004 and 2010, respectively. He studied metal coating techniques, fusion and solid-state welding methods, casting, and wear.